Nonlinear Analysis for Monitoring Bonded Patch Delamination

Mineyuki Nishino and Takahira Aoki

Department of Aeronautics and Astronautics, University of Tokyo, 7-3-1 Hongo, Bunkyo-ku, Tokyo 113-8656, Japan

ABSTRACT

A simple analytical model is developed to study the damaged patch structure, including the effect of large deflection. The method is based on the concept of equivalent delamination length, which is analytically defined and employed to describe load transfer between patch and parent plate with eccentrically aligned neutral axes. The analytical model has a closed form solution and good agreement with nonlinear finite element analysis (FEA) on deformation and energy release rate for parent plate crack and patch delamination is shown. The relation between the delamination propagation and the strains at monitoring locations is derived and feasibility of delamination monitoring based on surface strains is analytically demonstrated.

1. INTRODUCTION

Composite materials have been widely used for many years in aerospace industry because of its weight saving and other beneficial characteristics. Carbon fiber reinforced plastics (CFRP) structures are, like conventional metal structures, susceptible to damage which requires component replacement or repair. Considering economical efficiency and environmental concerns, repair is often desirable. Bonded repairs of composite structures are commonly adopted to restore the damaged structural components in compliance with the operational requirements. The bonded composite repair of metallic aircraft structures has been extensively studied experimentally and analytically [1].

In practical applications, unsymmetrical reinforcement of one-sided patch repair shown in Fig.1(a) is often adopted for the accessibility and other reasons. One-sided patch structure necessitates geometrically nonlinear analyses and thus the nonlinear FEA is commonly implemented. Closed form analytical models of one-sided patch structure have also been utilized. However, they do not adequately take into account the large deflection nature [2]. The geometrically nonlinear analytical model of patch delamination has also been studied, but it only covers the lap joints consisting of isotropic materials [3].

Monitoring technology of the original damage and bonded patch in the repaired structural integrity is strongly yearned for assuring safety robustness. Recently smart patches using

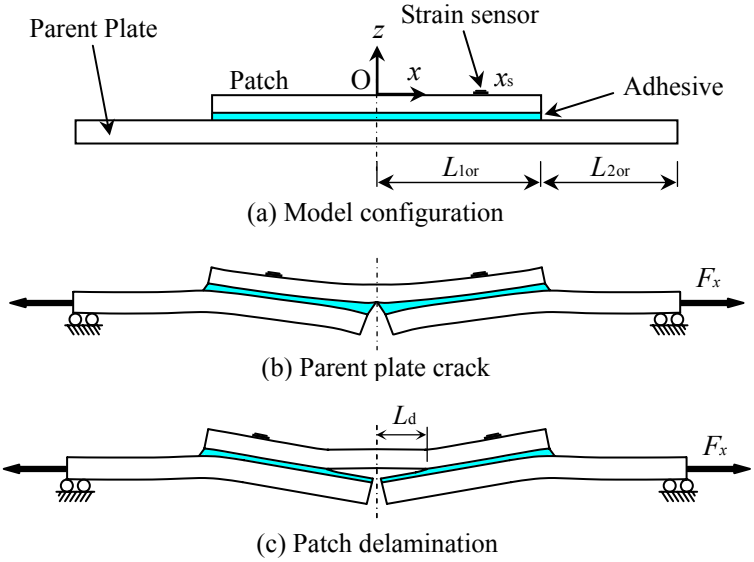

Fig.1. Cross section of composite patch repair

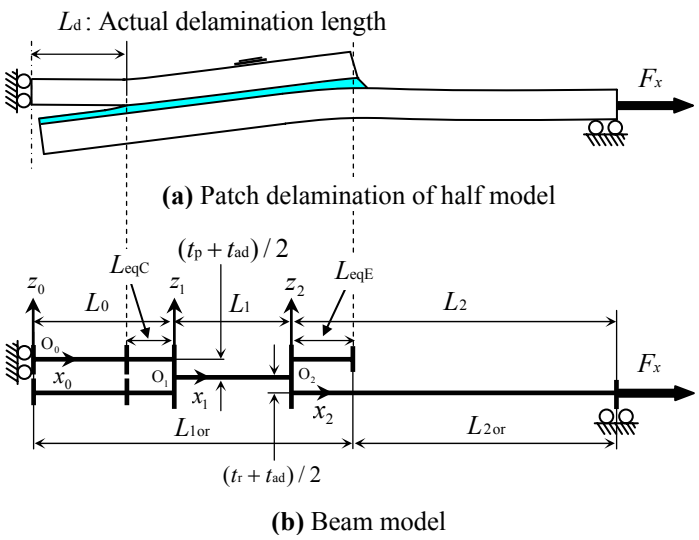

Fig.2. Beam model for patch delamination using equivalent delamination

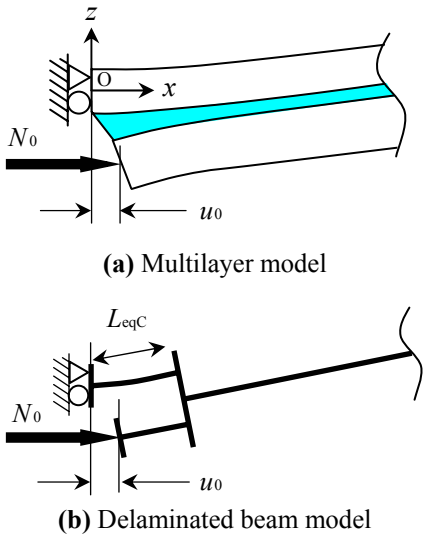

Fig.3. Derivation of equivalent delamination length

piezoelectric films or optical fibers have been brought to attention because of its capability of monitoring damages such as patch delamination [4].

In the present paper, the common one-sided patch structure consisting of CFRP bonded patch and the cracked CFRP parent plate is considered as shown in Fig.1(b). The patch is assumed herein to be $[0]_8$ unidirectional CFRP and the parent plate as $([45/0/-45/90]_s)_3$ quasi-isotropic laminate. The analysis of delaminated patch shown in Fig.1(c) under influence of the original plate crack is studied together with the strain monitoring of the patch surface associated with delamination propagation.

2. ANALYSIS

The original patched plate is shown in Fig.1(a). The composite patch of length $2L_{1or}$ is bonded to the composite parent plate of length $2(L_{1or}+L_{2or})$ with the adhesive. Under the axial tensile loading of F_x, there are multiple failure modes of the patched structure, *e.g.,* parent plate crack propagation, patch delamination, patch failure or cohesive failure. In this paper parent plate crack and patch delamination are considered as shown in Fig.1(b) and (c) respectively.

Considering the damaged patched structure such as the delaminated patch shown in Fig.1(c), the load transfer from the parent plate to the patch through the adhesive layer takes place near the delamination crack tip and the patch edge. Applying beam theory to this thin layered structure, the load transfer can be assumed to occur between the eccentrically aligned neutral axes. This eccentricity necessitates a geometrically nonlinear analysis [5,6].

The analytical model of patch repair must be developed incorporating the accurate load transfer, eccentrically aligned neutral axes and large deflection. The load transfer and the eccentricity is modeled as the equivalent delamination. The analytical model (beam model) consists of five longitudinal portions of Timoshenko beams; i.e. delaminated, equivalently delaminated, non-delaminated, equivalently delaminated and mere parent plate portions as shown in Fig.2(b). This figure illustrates the hypothetical delamination length (L_0) is longer than the actual length (L_d), the difference being the existence of the equivalent delamination length (L_{eqC}).

Figure 3 shows the derivation scheme of the equivalent delamination length. The equivalent delamination length is defined as the length of the delaminated beam model shown in Fig.3(b), where the crack opening displacement u_0 derived from the multilayer model shown in Fig.3(a) is identical to the one derived from the delaminated beam model. The multilayer model, where

the displacements of each layer are independent and the interaction between layers is modeled, will be described later in Section 2.2.

Nonlinear FEA is carried out in order to verify the analytical model, using NASTRAN commercial code. Four-noded plane element (QUAD4) is used with the total number of elements of about 8,000.

2.1 BEAM MODEL

The adhesive debonded patch structure shown in Fig.2(a) is modeled as Timoshenko beams incorporating large deflection and consists of three longitudinal portions (subscript); i.e. delaminated (0), nondelaminated (1) and mere parent plate portions (2) as shown in Fig.2(b). Each length is given by

$$L_0 = L_{\mathrm{d}} + L_{\mathrm{eqC}} \tag{1}$$

$$L_1 = L_{1\mathrm{or}} - (L_{\mathrm{d}} + L_{\mathrm{eqC}} + L_{\mathrm{eqE}}) \tag{2}$$

$$L_2 = L_{2\mathrm{or}} + L_{\mathrm{eqE}} \tag{3}$$

Under the Timoshenko beam hypothesis; i.e., straight lines perpendicular to the midline prior to deformation remain straight after deformation, the displacements of each portions are expressed as

$$u_i(z_i) = u_i(0) + z_i\psi_i \quad w_i(z_i) = w_i \quad i = 0,1,2 \tag{4}$$

The strains associated with the displacement Eq. 4 considering large deflection can be computed as

$$\varepsilon_{xi}(z_i) = \frac{du_i(0)}{dx_i} + \frac{1}{2}\left(\frac{dw_i}{dx_i}\right)^2 + z_i\frac{d\psi_i}{dx_i} \equiv \varepsilon_{0i} + z_i\kappa_i \tag{5}$$

$$\gamma_i = \psi_i + \frac{dw_i}{dx_i} \tag{6}$$

The displacement coincides with first-order laminate theories [7] subjected to cylindrical bending, thus the constitutive relations are written as

$$\begin{bmatrix} N \\ M \\ Q \end{bmatrix}_i = \begin{bmatrix} A_{11} & B_{11} & 0 \\ B_{11} & D_{11} & 0 \\ 0 & 0 & kA_{55} \end{bmatrix}_i \begin{bmatrix} \varepsilon_o \\ \kappa \\ \gamma \end{bmatrix}_i \tag{7}$$

where N_i are the axial resultant forces, M_i are the bending resultant moments, Q_i are the shear resultant forces and k is a shear correction factor. In addition

$$\left(A_{11_i}, B_{11_i}, D_{11_i}\right) = \int_{-t_i/2}^{t_i/2} Q_{11_i}\left(1, z_i, z_i^2\right) dz_i \tag{8}$$

$$A_{55_i} = \int_{-t_i/2}^{t_i/2} C_{55_i} dz_i \tag{9}$$

where Q_{11_i} are reduced stiffness coefficients for plane stress and C_{55_i} are shear stiffness coefficients.

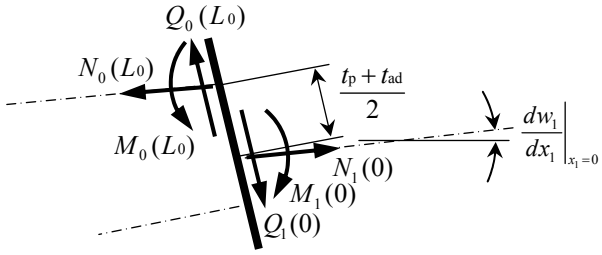

Fig.4. Continuity conditions at $x_0 = L_0 (x_1 = 0)$

The equilibrium equations are of the form

$$\frac{dN_i}{dx_i} = 0 \quad (N_i = F_x \text{(const.)}) \tag{10}$$

$$\frac{dQ_i}{dx_i} + \frac{d}{dx_i}\left(N_i \frac{dw_i}{dx_i}\right) = 0 \tag{11}$$

$$\frac{dM_i}{dx_i} - Q_i = 0 \tag{12}$$

The three portions are interconnected satisfying the geometrical and mechanical continuity conditions, with the eccentricities between their neutral axes taken into account. Figure 4 illustrates the continuity conditions at the interface $x_0 = L_0 (x_1 = 0)$;

$$w_0(L_0) = w_1(0) \quad \psi_0(L_0) = \psi_1(0) \tag{13}$$

$$F_x \frac{t_p + t_{ad}}{2} + M_0(L_0) = M_1(0) \tag{14}$$

$$Q_0(L_0) + F_x \left.\frac{dw_0}{dx_0}\right|_{x_0 = L_0} = Q_1(0) + F_x \left.\frac{dw_1}{dx_1}\right|_{x_1 = 0} \tag{15}$$

Combining the strain-displacement relations Eqs. 5 and 6, the constitutive relations Eq. 7 and the equilibrium equations Eqs. 10 - 12, the following governing equations are obtained

$$\frac{d^2 w_i}{dx_i^2} = \alpha_i^2 \left(w_i - C_{1i} x_i - C_{2i}\right) \tag{16}$$

where C_{1i} and C_{2i} are integral constants and

$$\alpha_i^2 = \frac{1}{1/kA_{55_i} + 1/F_x} \frac{1}{D_{11_i} - B_{11_i}^2 / A_{11_i}} \tag{17}$$

The general solutions of Eq. 16 are calculated as

$$w_i = A_i \sinh \alpha_i x_i + B_i \cosh \alpha_i x_i + C_{1i} x_i + C_{2i} \tag{18}$$

where A_i and B_i are constants derived from the boundary and continuity conditions.

The energy release rate is generally defined as

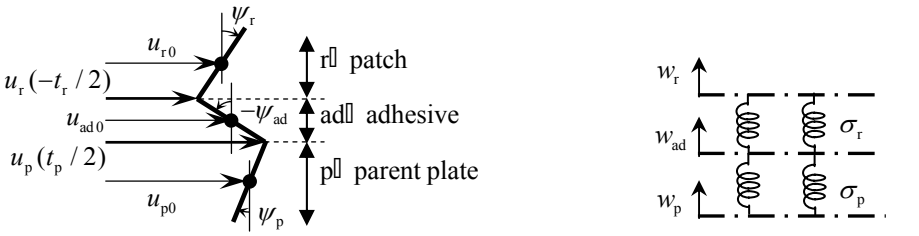

(a) Inplane displacements at interface **(b)** Peel stresses at interface

Fig.5. Continuity conditions of multilayer model

$$G = -\frac{\partial \Pi}{\partial a} \tag{19}$$

where Π is the potential energy per width and a is the crack length. The energy release rate associated with parent plate crack shown in Fig.1(b) is expressed as

$$G = -\frac{\Delta \Pi}{t_p + t_{ad}} \tag{20}$$

where $\Delta\Pi$ is the difference of the potential energy per width between the intact patched structure and the parent plate cracked structure shown in Fig.1(b). The energy release rate due to the patch delamination shown in Fig.1(c) is expressed as

$$G = -\frac{\partial \Pi}{\partial L_d} \tag{21}$$

2.2 MULTILAYER MODEL

The crack opening displacement u_0 shown in Fig.3(a) is calculated from the multilayer model under the assumption of geometrically linear condition. Similar to Eq. 4 the inplane displacements of patch, parent plate and adhesive are given by

$$\begin{aligned} &\text{Patch:} && u_r(z_r) = u_{r0} + z_r\psi_r \\ &\text{Parent plate:} && u_p(z_p) = u_{p0} + z_p\psi_p \\ &\text{Adhesive:} && u_{ad}(z_{ad}) = u_{ad0} + z_{ad}\psi_{ad} \end{aligned} \tag{22}$$

Assuming the continuity conditions of the inplane displacements at the interface as shown in Fig.5(a), the inplane displacements of the adhesive are expressed using the inplane displacements of patch and parent plate as

$$\begin{aligned} u_{ad0} &= \frac{u_r(-t_r/2) + u_p(z_p/2)}{2} = \frac{u_{r0} + u_{p0}}{2} + \frac{-t_r\psi_r + t_p\psi_p}{4} \\ \psi_{ad} &= \frac{u_r(-t_r/2) - u_p(z_p/2)}{t_{ad}} = \frac{u_{r0} - u_{p0}}{t_{ad}} - \frac{t_r\psi_r + t_p\psi_p}{2t_{ad}} \end{aligned} \tag{23}$$

On the other hand, deflections w_r, w_{ad}, w_p are defined independently. The strains can also be obtained similarly where linear strain-displacement relations are considered.

Integrating the strain energy density φ_i in the thickness direction of each layer, one obtains

$$U_i = \int_{-t_i/2}^{t_i/2} \varphi_i dz_i = \frac{1}{2}\left(A_{11_i} {\varepsilon_{i0}}^2 + 2B_{11_i}\varepsilon_{i0}\kappa_i + D_{11_i}{\kappa_i}^2 + kA_{55_i}{\gamma_i}^2 \right) \tag{24}$$

In Eq. 24, the strain energy associated with the extension in the thickness direction is not considered because of the Timoshenko beam hypothesis. Therefore the strain energy is separately taken into account as

$$U_w = \frac{1}{2}k_{\mathrm{ad_r}}\left(w_{\mathrm{r}} - w_{\mathrm{ad}}\right)^2 + \frac{1}{2}k_{\mathrm{ad_p}}\left(w_{\mathrm{ad}} - w_{\mathrm{p}}\right)^2 \tag{25}$$

where $k_{\mathrm{ad_r}}$ and $k_{\mathrm{ad_p}}$ are parameters associated with extensional rigidity in the thickness direction. The total potential energy per width Π of the system of longitudinal length l is

$$\Pi = \int_0^l \left(U_{\mathrm{r}} + U_{\mathrm{ad}} + U_{\mathrm{p}} + U_{\mathrm{w}}\right) dx + \Phi \tag{26}$$

where Φ is the potential energy of external forces and x is the global coordinate defined in Fig.3(a). According to the principle of minimum potential energy, the variation of the total potential energy with respect to the admissible displacements leads to the equilibrium equations and mechanical boundary conditions [8]. The equilibrium equations are derived as

$$\begin{cases} \delta u_{\mathrm{r0}} : \dfrac{dN_{\mathrm{r}}}{dx} + \dfrac{1}{2}\dfrac{dN_{\mathrm{ad}}}{dx} + \dfrac{1}{t_{\mathrm{ad}}}\left(\dfrac{dM_{\mathrm{ad}}}{dx} - Q_{\mathrm{ad}}\right) = 0 \\ \delta u_{\mathrm{p0}} : \dfrac{dN_{\mathrm{p}}}{dx} + \dfrac{1}{2}\dfrac{dN_{\mathrm{ad}}}{dx} - \dfrac{1}{t_{\mathrm{ad}}}\left(\dfrac{dM_{\mathrm{ad}}}{dx} - Q_{\mathrm{ad}}\right) = 0 \end{cases} \tag{27}$$

$$\begin{cases} \delta\psi_{\mathrm{r}} : \dfrac{dM_{\mathrm{r}}}{dx} - Q_{\mathrm{r}} - \dfrac{t_{\mathrm{r}}}{2}\left\{\dfrac{1}{2}\dfrac{dN_{\mathrm{ad}}}{dx} + \dfrac{1}{t_{\mathrm{ad}}}\left(\dfrac{dM_{\mathrm{ad}}}{dx} - Q_{\mathrm{ad}}\right)\right\} = 0 \\ \delta\psi_{\mathrm{p}} : \dfrac{dM_{\mathrm{p}}}{dx} - Q_{\mathrm{p}} + \dfrac{t_{\mathrm{p}}}{2}\left\{\dfrac{1}{2}\dfrac{dN_{\mathrm{ad}}}{dx} - \dfrac{1}{t_{\mathrm{ad}}}\left(\dfrac{dM_{\mathrm{ad}}}{dx} - Q_{\mathrm{ad}}\right)\right\} = 0 \end{cases} \tag{28}$$

$$\begin{cases} \delta w_{\mathrm{r}} : \dfrac{dQ_{\mathrm{r}}}{dx} - \sigma_{\mathrm{r}} = 0 \\ \delta w_{\mathrm{ad}} : \dfrac{dQ_{\mathrm{ad}}}{dx} + \sigma_{\mathrm{r}} - \sigma_{\mathrm{p}} = 0 \\ \delta u_{\mathrm{p0}} : \dfrac{dQ_{\mathrm{p}}}{dx} + \sigma_{\mathrm{p}} = 0 \end{cases} \tag{29}$$

where the resultant forces are identical to ones defined in Eq. 7. In addition the peel stresses shown in Fig.5(b) are defined as

$$\begin{aligned} \sigma_{\mathrm{r}} &= k_{\mathrm{ad_r}}\left(w_{\mathrm{r}} - w_{\mathrm{ad}}\right) \\ \sigma_{\mathrm{p}} &= k_{\mathrm{ad_p}}\left(w_{\mathrm{ad}} - w_{\mathrm{p}}\right) \end{aligned} \tag{30}$$

The general boundary conditions are derived as

$$\overline{N_{\mathrm{r}}} = N_{\mathrm{r}} + \frac{1}{2}N_{\mathrm{ad}} + \frac{1}{t_{\mathrm{ad}}}M_{\mathrm{ad}} \qquad \text{or} \qquad \overline{u_{\mathrm{r0}}} = u_{\mathrm{r0}} \tag{31}$$

$$\overline{N_{\mathrm{p}}} = N_{\mathrm{p}} + \frac{1}{2}N_{\mathrm{ad}} - \frac{1}{t_{\mathrm{ad}}}M_{\mathrm{ad}} \qquad \text{or} \qquad \overline{u_{\mathrm{p0}}} = u_{\mathrm{p0}} \tag{32}$$

$$\overline{M_{\mathrm{r}}} = M_{\mathrm{r}} - \frac{t_{\mathrm{r}}}{2}\left(\frac{1}{2}N_{\mathrm{ad}} + \frac{1}{t_{\mathrm{ad}}}M_{\mathrm{ad}}\right) \qquad \text{or} \qquad \overline{\psi_{\mathrm{r}}} = \psi_{\mathrm{r}} \tag{33}$$

$$\overline{M_{\mathrm{p}}} = M_{\mathrm{p}} + \frac{t_{\mathrm{p}}}{2}\left(\frac{1}{2}N_{\mathrm{ad}} - \frac{1}{t_{\mathrm{ad}}}M_{\mathrm{ad}}\right) \qquad \text{or} \qquad \overline{\psi_{\mathrm{p}}} = \psi_{\mathrm{p}} \tag{34}$$

$$\overline{Q_{\mathrm{r}}} = Q_{\mathrm{r}} \qquad \text{or} \qquad \overline{w_{\mathrm{r}}} = w_{\mathrm{r}} \tag{35}$$

$$\overline{Q_{\mathrm{ad}}} = Q_{\mathrm{ad}} \qquad \text{or} \qquad \overline{w_{\mathrm{ad}}} = w_{\mathrm{ad}} \tag{36}$$

$$\overline{Q_{\mathrm{p}}} = Q_{\mathrm{p}} \qquad \text{or} \qquad \overline{w_{\mathrm{p}}} = w_{\mathrm{p}} \tag{37}$$

In case of the system as shown in Fig. 3(a), in which the axial force N_0 is acting at the neutral axis of the parent plate, the boundary conditions at $x = 0$ are given by

$$\overline{u_{\mathrm{r0}}} = \overline{\psi_{\mathrm{r}}} = \overline{w_{\mathrm{r}}} = 0 \tag{38}$$

$$\overline{N_{\mathrm{p}}} = -N_0 \tag{39}$$

$$\overline{M_{\mathrm{p}}} = -N_0\,\overline{B_{11_{\mathrm{p}}}} \tag{40}$$

$$\overline{Q_{\mathrm{p}}} = \overline{Q_{\mathrm{ad}}} = 0 \tag{41}$$

where

$$\overline{B_{11_{\mathrm{p}}}} = B_{11_{\mathrm{p}}} / A_{11_{\mathrm{p}}} \tag{42}$$

The governing equations related to the adhesives have to be derived as follows. Differentiating Eq. 23 with respect to *x*, one obtains the continuity conditions of strains at the upper and lower adhesive interface

$$\begin{aligned} \varepsilon_{\mathrm{ad0}} + \frac{t_{\mathrm{ad}}}{2}\kappa_{\mathrm{ad}} &= \varepsilon_{\mathrm{r0}} - \frac{t_{\mathrm{r}}}{2}\kappa_{\mathrm{r}} \\ \varepsilon_{\mathrm{ad0}} - \frac{t_{\mathrm{ad}}}{2}\kappa_{\mathrm{ad}} &= \varepsilon_{\mathrm{p0}} + \frac{t_{\mathrm{p}}}{2}\kappa_{\mathrm{p}} \end{aligned} \tag{43}$$

Combining strain-displacement relations, equilibrium equations and Eq. 43, one arrives at the governing equations with respect to peel stresses

$$\begin{bmatrix} \sigma_{\mathrm{r}} \\ \sigma_{\mathrm{p}} \end{bmatrix}^{(4)} + \begin{bmatrix} a_{11} & a_{12} \\ a_{21} & a_{22} \end{bmatrix} \begin{bmatrix} \sigma_{\mathrm{r}} \\ \sigma_{\mathrm{p}} \end{bmatrix}^{(2)} + \begin{bmatrix} b_{11} & b_{12} \\ b_{21} & b_{22} \end{bmatrix} \begin{bmatrix} \sigma_{\mathrm{r}} \\ \sigma_{\mathrm{p}} \end{bmatrix} = \begin{bmatrix} 0 \\ 0 \end{bmatrix} \tag{44}$$

where a_{ij}, b_{ij} are constants. Although the order of the characteristic equation of Eq. 44 is 8, only the even order terms exist, therefore the Eq. 44 has closed form solutions. Presuming all stresses to dissipate as $x \to \infty$, one obtains the general solutions

$$\begin{cases} \sigma_{\mathrm{r}} = \sum_{i=1}^{4} C_i \, \mathrm{e}^{-\lambda_i x} \\ \sigma_{\mathrm{p}} = \sum_{i=1}^{4} \overline{C_i} \, \mathrm{e}^{-\lambda_i x} \end{cases}, \qquad \begin{cases} \sigma_{\mathrm{r}} = \sum_{i=1}^{2} C_i \, \mathrm{e}^{-\lambda_i x} + \mathrm{e}^{-\lambda_3 x}\left(C_3 \sin \lambda_4 x + C_4 \cos \lambda_4 x\right) \\ \sigma_{\mathrm{p}} = \sum_{i=1}^{2} \overline{C_i} \, \mathrm{e}^{-\lambda_i x} + \mathrm{e}^{-\lambda_3 x}\left(\overline{C_3} \sin \lambda_4 x + \overline{C_4} \cos \lambda_4 x\right) \end{cases} \tag{45}$$

Table 1. Material properties of patch structure.

Material	Young's modulus(GPa)	Poisson' s ratio
Adhesive	1.89	0.33
CFRP	E_L: 147.1, E_T : 8.310 G_{LT}: 4.707, G_{TT}: 2.866	0.352(ν_{LT})

Table 2. Model configuration of patch structure.

Stacking sequence		Thickness [mm]			Length [mm]	
Patch	Parent Plate	Patch	Adhesive	Parent plate	L_{1or}	L_{2or}
$[0]_8$	$([45/0/-45/90]_s)_3$	1.0	0.1	3.0	60.0	300.0

where C_i and $\overline{C}_i$ are constants derived from the boundary conditions. For most of the composite patch of interest, solution □ should be employed.

3. RESULTS

A typical patch specimen made of CFRP and adhesive was chosen to verify the validity of the model. The material properties and configuration of the specimen are listed in Table 1 and 2 respectively.

Deformation of neutral axes at delamination length of $L_d / L_{1or} = 0.5$ under the axial tensile loading of 100 [MPa] is plotted in Fig.6 together with their initial locations. Vertical axis is normalized with the distance of the neutral axis z_{n02} between the delaminated patch portion and mere parent plate portion. This figure illustrates the behavior of one-sided patch, in which each neutral axis is asymptotically aligned, and the large deflection compared to the thickness indicates the necessity of considering large deflection effect.

Surface strain distributions with delamination length of $L_d / L_{1or} = 0.5$ under tensile loading of 100 [MPa] are shown in Fig.7, normalized with the strain of the independently elongated patch. The strains calculated from the analytical model are almost identical to the results from the FEA except for the vicinity of the edge of the patch and the delamination crack tip. The good agreement implies the validity of the analytical model.

The energy release rate due to the plate crack defined by Eq. 20 under tensile loading of 100 [MPa] is plotted in Fig.8 as a function of the half patch length. The energy release rate is calculated both from analytical model and FEA, assuming geometrically linearity and nonlinearity. The considerable difference between the linear and nonlinear results indicates the necessity of nonlinear analysis.

Considering patch delamination of half model, two modes of delamination which are crack tip patch delamination and patch edge delamination are of interet as shown in Fig.9. Comparison of extension of the existing crack tip patch delamination and initiation of patch edge delamination in terms of energy release rate under tensile loading of 100 [MPa] is made as functions of crack tip patch delamination length (Fig.9). The energy release rates are calculated from geometrically nonlinear analytical model and nonlinear FEA. The energy release rate due to the crack tip patch delamination is always larger than one due to the patch edge delamination. This result leads to the possibility of the crack tip patch delamination rather than the patch edge delamination, and thus the former is considered throughout this paper and called hereafter as "patch delamination".

The relation between delamination propagation and the strain output of the sensors s_0, s_1 shown in Fig.10(a) at the patch surface is plotted in Fig.10(b). The results are obtained from the analytical model and FEA under the axial tensile loading of 100 [MPa] and again normalized with the uniform patch strain when loaded independently. This figure illustrates

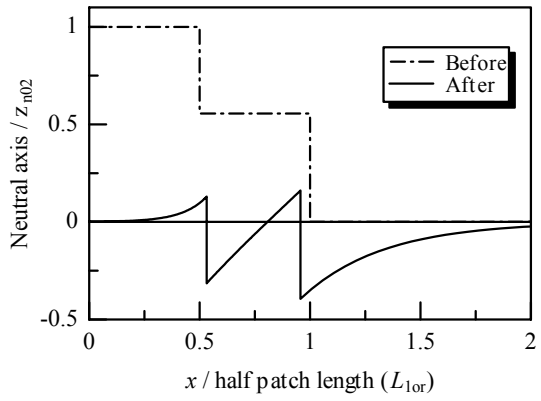

Fig.6. Deformation of neutral axes at delamination length of $L_d / L_{1or} = 0.5$

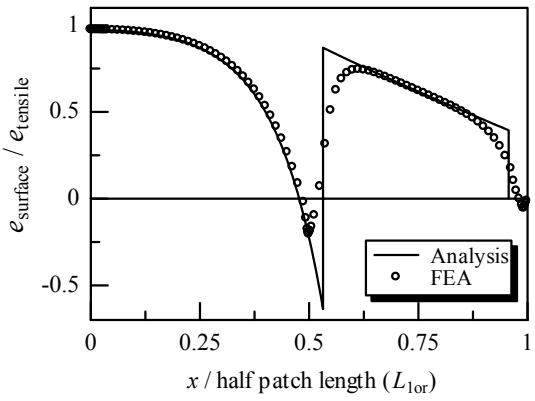

Fig.7. Patch surface strain distributions at delamination length of $L_d / L_{1or} = 0.5$

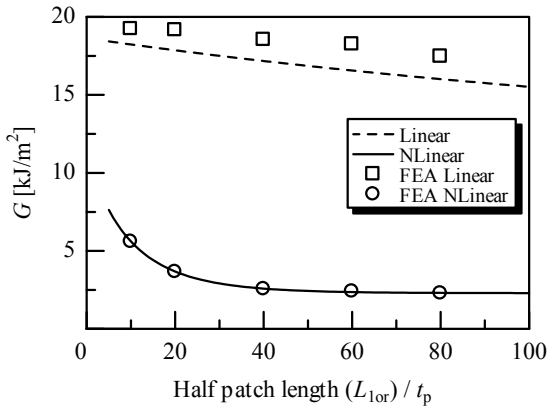

Fig.8. Energy release rate due to parent plate crack versus half patch length (100 [MPa] tensile loading)

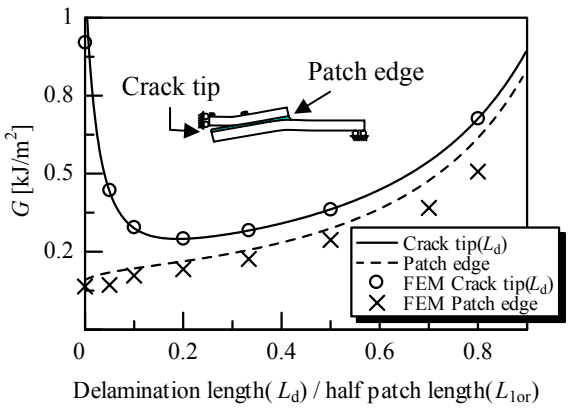

Fig.9. Energy release rate for crack tip patch delamination extension and patch edge delamination initiation versus crack tip patch delamination length (L_d) (100 [MPa] tensile loading)

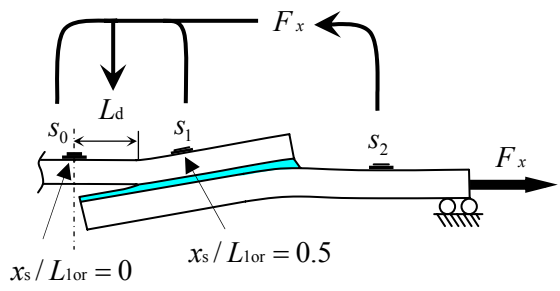

(a) Sensor locations and monitoring strategy

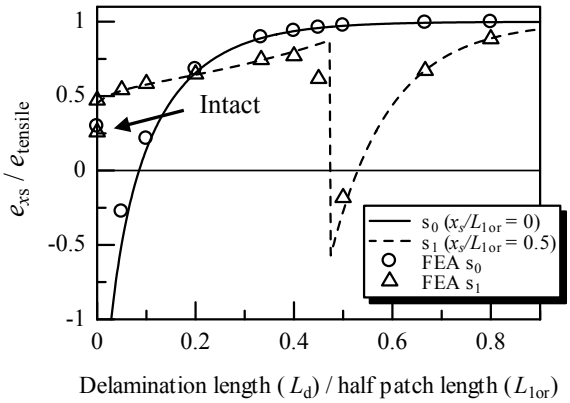

(b) Strains(e_{xs}) at monitoring locations for patch delamination (x_s are x-coordinates of monitoring locations)

Fig.10. Damage monitoring based on surface strains

the response of the two sensors to patch delamination. Even when the delamination doesn't reach the strain-monitoring location, the strain increases as delamination propagates. On the other hand, when the delamination propagates through the monitoring location, the strain shows a sharp decline down to negative value. The strain increases again to the asymptotic value, which represents the uniformly elongated state without bending.

When the strain is monitored with s_1 (dashed line), the normalized strain is about 0.5 without delamination and increasing up to 0.75 as delamination propagates, suggesting the possibility of practically detecting delamination propagation. Noting that the normalized strain level of intact patch structure with no crack is about 0.25, which goes up to 0.5 with crack introduction, the detection of crack propagation in the parent plate may also be possible.

The damage monitoring strategy of the half model based on the three surface strain sensors; s_0, s_1, s_2 is shown in Fig.10(a). First the axial tensile loading is estimated based on the strain sensor s_2, which is placed far from the overlap end where almost uniformly elongated state without bending is realized. Second the relation between delamination propagation and the strains at the sensors s_0, s_1 is calculated. Finally delamination length is founded by solving the relation inversely.

4. CONCLUTIONS

The delaminated one-sided patch-repaired plate was modeled as combination of Timoshenko beams consisting of three portions in which large deflection and eccentrically aligned neutral axes are taken into account. The analytical model was based on the concept of equivalent delamination and had a closed form solution. The results showed good agreement with nonlinear FEA except at the boundary region.

The relation between the delamination propagation and the strains at monitoring locations was shown and feasibility of delamination monitoring based on surface strains was analytically demonstrated.

ACKNOWLEDGEMENTS

One of the authors (M.N.) was supported through the 21st Century COE Program, "Mechanical Systems Innovation," by the Ministry of Education, Culture, Sports, Science and Technology.

References

1. **Baker,A.A**., **Rose, L.R.F.** and **Jones, R.**, *Eds*., Advances in the Bonded Composite Repair of Metallic Aircraft Structure, Elsevier, 2002.
2. **Rose., L.R.F.** and **Wang., C.H.**, 'Advances in the Bonded Composite Repair of Metallic Aircraft Structure,' in A.A. Baker, L.R.F. Rose, and R. Jones, *Eds*., "Analytical Methods for Designing Composite Repairs", Chapter 7, Elsevier, 2002.
3. **Lai., Y.H.**, **Rakestraw., M.D.** and **Dillard., D.A.**, "The Cracked Lap Shear Specimen Revisited – A Closed Form Solution," *Int. J. Solids and Structures*, Vol.33, No.12(1996), pp.1725-1743.
4. **McKebzie.**, **I., Jones., R.**, **Marshall., I.H.** and **Galea., S.**, "Optical fibre sensors for health monitoring of bonded repair systems", *Composite Structures*, **50**(2000), 405-416.
5. **Klug., J.C.** and **Sun., C.T.,** "Large deflection effects of cracked aluminium plates repaired with bonded composite patches", *Composite Structures*, **42**(1998), 291-296.
6. **Umamaheswar., T.V.R.S.** and **Singh., R.**, "Modelling of a patch repair to a thin cracked sheet", *Eng. Fract. Mech.*, **62**(1999), 267-289.
7. **Reddy, J.N.**, Mechanics of Laminated Composite Plates, CRC Press, 1997.
8. **Washizu, K.,** Variational methods in elasticity and plasticity second edition, Pergamon Press, 1975.